Two-nucleon absorption of π^+ in ^{4}He at $T_{\pi+}$ = 114 and 162 MeV

F. Adimi, H. Breuer, B. S. Flanders,* M. A. Khandaker,† M. G. Khayat, P. G. Roos, and D. Zhang‡
Department of Physics, University of Maryland College Park, Maryland 20742

Th. S. Bauer§ and J. Konijn
Nationaal Instituut voor Kernfysica en Hoge-Energiefysica, Postbus 4395, NL 1009 AJ Amsterdam, The Netherlands

C. T. A. M. de Laat
Physics Laboratory, University Utrecht, Postbus 80000, 3508 TA Utrecht, The Netherlands

G. S. Kyle, S. Mukhopadhyay, and M. Wang
Department of Physics, New Mexico State University, Las Cruces, New Mexico 88003

R. Tacik**
University of Karlsruhe, 7500 Karlsruhe, Federal Republic of Germany
(Received 12 February 1992)

Differential and integrated cross sections for the reaction ^{4}He(π^+, pp) at T_π=114 and 162 MeV are reported. These are the first results for this reaction using a large solid angle detector covering ≈55% of 4π sr. Directly measured integrated cross sections for absorption on two-nucleon pairs are σ_{abs} = 25.7±1.8 mb at 114 MeV and σ_{abs} = 21.0±1.5 mb at 162 MeV. These cross sections, when corrected by a factor of 1.4 for final-state interaction effects, account for about 50% of the total absorption cross section for all final state reaction channels at both energies. The data are compared with Monte Carlo simulations of the reaction process using a quasideuteron absorption model for the two-nucleon absorption process in a plane wave impulse approximation. The consequences for the extraction of the two-nucleon absorption cross section by imposing different conditions on the data are explored.

PACS number(s): 25.80.Ls, 25.80.-e, 27.10.+h, 21.45.+v

I. INTRODUCTION

Pion absorption on light nuclei has been studied extensively in recent years (see, for example, Ref. [1] for a recent review). Despite the importance of absorption in the pion-nucleus interaction, theoretically it is one of the least understood reactions of pions with nuclei. High quality absorption data on deuterium [2] and ^{3}He [3–6], as well as some measured and deduced cross sections for heavier targets such as ^{6}Li [7, 8], ^{12}C [9], ^{16}O [10–13], and ^{58}Ni [14], over a broad range of energies near the Δ-resonance exist in the literature. However, a paucity of quality data exists for the nucleus ^{4}He which is of special interest for pion absorption. Compared to ^{2}H and ^{3}He, ^{4}He has several of the properties of heavier nuclei [e.g., increased nuclear density, large binding energy per nucleon, and the absorption of a pion can result in multibody (> 3) final states], while the experimental complications of heavy nuclei (e.g., nuclear structure details and multistep reaction processes) are kept to a minimum. Moreover, the A dependence of the total absorption cross section for $A \geq 4$ can be fitted by a power law [9], whereas the cross sections for ^{2}H and ^{3}He fall well below such a curve. These results suggest that a change in the modes of absorption, possibly involving more than two nucleons, takes place near A=4. Because of the reduced probability for multistep processes, ^{4}He becomes an ideal nucleus with which to study the absorption of pions by nuclei. Existing data for pion absorption in ^{4}He [15–20] are not of sufficient accuracy or completeness to separate the various dependences of pion interactions on the nuclear parameters mentioned above.

A recent study of pion absorption on ^{4}He at T_π=120 MeV [19] provides an overview of all final-state reaction channels. However, the absolute cross sections are rather

*Present address: Dept. of Physics, American University, Washington, D.C. 20016.
†Present address: Dept. of Physics, Virginia Polytechnic Institute & State University, Blacksburg, VA 24061, and Physics Dept., Brookhaven National Laboratory, Upton, NY 11973.
‡Present address: Petrophysical Engineering, Shell Development, P.O. Box 482, Houston, TX 77001.
§Present address: Physics Laboratory, University Utrecht, P.O. Box 80000, 3508 TA Utrecht, The Netherlands.
**Present address: Dept. of Physics, University of Regina, Regina, SK S4S OA2, Canada.

uncertain (about ±20%). Also, past studies of pion absorption on ^{4}He have been performed with limited solid angle detectors exploring only certain kinematic regions of the multibody final states. This necessitated extensive extrapolations into the unmeasured regions of phase space using model-dependent assumptions about the distribution of reaction products in phase space to obtain cross sections.

A major fraction of the absorption cross section in the region of the Δ resonance involves the absorption of a pion by a proton-neutron pair [3–14] (two-nucleon absorption, 2NA). Furthermore, experimental evidence [5, 6, 18, 19, 21] as well as theoretical arguments and calculations [22, 23] indicate that absorption on $^3S_1(T = 0)$ pairs dominates the 2NA process, whereas absorption on $^1S_0(T = 1)$ pairs is very weak. Such observations naturally led to the formulation of a quasideuteron absorption (QDA) model. The QDA model has been quite successful in describing many aspects of the experimental data (see, for example, Ref. [10] and references therein) by assuming that the absorption process takes place on a pair of nucleons (with Fermi momentum) in the nucleus having the same initial quantum numbers as those of a physical deuteron [18] ($T = 0, S = 1$). However, this assumption has not been tested over the full range of all kinematic variables. Indeed, compared to deuterium, the presence of additional nucleons in ^{4}He and its increased nuclear density are expected to modify the QDA cross section compared to that of the free deuterium [23, 24]. Thus, questions remain as to the absolute value of the 2NA and QDA cross sections in ^{4}He and the quantitative details of the distribution of reaction products in phase space as compared to distributions obtained from absorption on a deuteron.

In this paper we report first results for π^+ absorption on ^{4}He covering most of the possible angle combinations of the two-nucleon angular correlations allowing a quantitative test of these aspects of the QDA model. The detector setup allowed us to integrate these angular correlations with little extrapolation into the unmeasured regions of phase space. Our results at two incident pion energies across the peak of the Δ resonance allow us to explore the energy dependence of 2NA with very small relative uncertainties.

II. EXPERIMENT AND ANALYSIS

A. Experimental details

The experiment was carried out at the πM1 channel of the Paul Scherrer Institut in Switzerland. Secondary beams of 114 and 162 MeV π^+ with an accepted momentum byte of ±1.5% were used to study in-flight pion absorption on a liquid ^{4}He target. Figure 1 shows a horizontal cut through the relevant elements of the experimental setup. The details of the cylindrical target of 30 mm diameter and its support assembly are described in detail elsewhere [25]. This target with its support structure was optimized for large solid angle coverage. A plastic scintillator (T1 in Fig. 1) in the beam defined an active interaction area 20 mm wide and 40 mm high. The target was surrounded by 16 plastic scintillator ΔE-E detector telescopes (ΔE, 10×200×1020 mm^3; E, 180×180×1000 mm^3) forming approximately a vertical cylinder with openings for the entrance and exit of the beam (Fig. 1, see also Refs. [25] and [26]). The scintillation light in the detectors, read out with photomultiplier tubes from both ends of each detector, provided energy, time-of-flight, and position information for the reaction fragments. The detectors were arranged to cover approximately equal solid angles in the center-of-mass system for 115 MeV pion absorption on deuterium. Thus, the ΔE detectors were located at distances varying between 477 and 710 mm from the target covering in-plane angles from 7° to 157°, and out-of-plane angles (measured perpendicular to the horizontal symmetry plane of the setup in Fig. 1) of ±35° to ±46° covering 55.4% of 4π sr. The E detectors were mounted 30 mm behind the ΔE detectors.

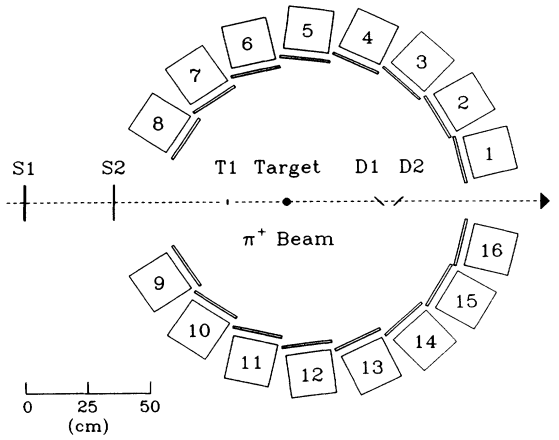

FIG. 1. A cut through the horizontal (in the laboratory system) symmetry plane of the experimental setup. The pion beam traverses a set of beam defining scintillators (S1, S2, and T1), followed by the cylindrical liquid ^{4}He target and two deuterated scintillators (D1, D2) used for calibrations. The 16 scintillator telescopes, consisting of one ΔE and E detector each, extend for 0.5 m each above and below the plane shown.

The out-of-plane acceptance in the current analysis was limited to ±400 mm on the ΔE detectors (i.e., ±30° to ±40°) in order to minimize the out-scattering effects from the ends of the E detectors. Taking into account that the properties of the reactions do not depend on rotations about the beam axis, this physical arrangement with the applied software limits covers more than 80% of any single-particle angular distribution and about 68% of all possible angular correlations for two particles. In the final software analysis of the data, the thresholds for particle detection were set to 6 MeV of deposited energy corresponding to reaction fragments with 18 MeV (protons) or 24 MeV (deuterons) at the target center.

The incident pion beam was defined and counted by the beam telescope consisting of plastic scintillators S1, S2, and T1 (Fig. 1) placed upstream of the target, pro-

viding the start signal for the time-of-flight (TOF) measurement of the reaction fragments. Nonpion contaminations of the beam (8% at 114 MeV) were identified by their TOF and momentum through the magnetic system of the beam line and by their energy losses in the beam scintillators. Typical pion flux rates on target were below 200 kHz—very low compared to the rf microstructure of the beam of 50 MHz. Thus, multiple pions in a single rf burst and pileup were neglegible.

Empty target runs were performed and the resulting spectra were subtracted in the later analysis. For the case A cross sections discussed later, the empty target events contributed about 5% to the yield. A cylindrical heavy water target (D_2O) of 7 mm diameter [26] (with 5×40 mm^2 beam-target overlap defined by two scintillators, T1 and an additional T2) was periodically placed at the He target position for calibration purposes. Also, two deuterated scintillators, D1 and D2, were placed permanently in the beam, downstream of the target. Pion absorption on the deuterium in these scintillators provided a continuous monitor of the gain in the photomultiplier tubes on the plastic detectors. To calibrate the position, obtained from the time difference from both ends of each detector, data were taken with a pair of iron absorbers located in front of each telescope.

B. Analysis, calibration, and resolution

Particle identification of the reaction fragments was achieved in two different ways. For all fragments the mass was calculated from TOF and kinetic energy. A typical ungated mass spectrum is shown in Fig. 2(a). Peaks corresponding to pions, protons, and deuterons are easily recognized. For reaction fragments with sufficient range (i.e., protons with more than approximately 38 MeV) their mass and charge has also been determined via the ΔE-E method, giving redundant particle identification for these fragments. Such an ungated spectrum is shown in Fig. 3(a). The same peaks are visible as in Fig. 2(a).

The kinetic energy of the reaction fragments was determined for high energy particles from the light collected in the scintillators. Since the particle masses are discrete quantities, the TOF can be used a second time in combination with the exact particle mass to obtain the kinetic energy. For energies below about 50 MeV, this TOF generated energy was combined with the energy obtained from light to improve the energy resolution. Tables were generated containing the average energy lost in nondetector material for each particle type as a function of the energy detected. These missing energies have been added event by event to yield the particle energy at the point of reaction. The success of the energy calibration for the full range of kinetic energies can be judged from the straightness of the proton mass line in Fig. 4 and by the mass values obtained for deuterons.

Figure 4 also shows the effects on mass identification for events that did not deposit their full kinetic energy as light output. Since the ΔE detectors are wider than the E detectors, some protons have only a ΔE signal. This results in the diagonal band joining the proton band

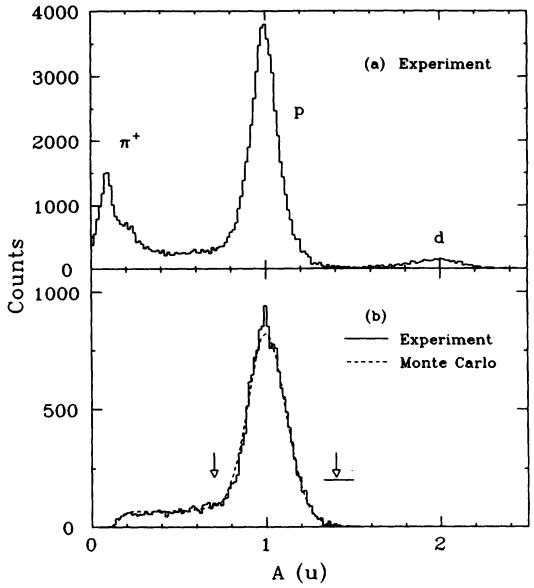

FIG. 2. The mass, A, identification using the TOF and kinetic energy for fragments detected in telescope 3 after the absorption of 114 MeV pions. The peaks in (a), from left to right, correspond to pions, protons, and deuterons. In (b) the same data are shown after requiring an additional coincident proton in telescope 11 or 12. The low mass tail is due to imperfect kinetic-energy collection. The normalized QDA-MC simulation data are shown as the dashed line. An event must be located between the limits indicated by the arrows to be accepted as a proton. The upper limit is energy dependent, as indicated by the horizontal range below the arrow.

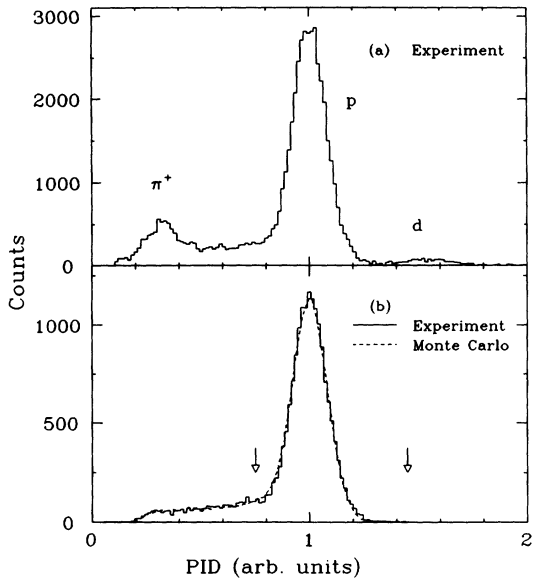

FIG. 3. Mass identification (PID) using the ΔE-E method for events penetrating into the E detector of telescope 3 after the absorption of 114 MeV pions. Peaks for pions, protons, and deuterons are indicated. In (b) the same gates as in Fig. 2(b) have been applied and the arrows have equivalent meaning.

near 35 MeV. In addition, protons entering the E detector may escape through the detector sides ("punch-through") or dissipate some undetected kinetic energy in a nuclear reaction in the detector. Both of these effects are energy dependent and are roughly equal in magnitude for this experiment. Such events create the diagonal band at high energies joining the proton band at the peak of the yield near 130 MeV. The remaining non-proton peaks in Fig. 4 are due to pions ($A \approx 0.2$) and deuterons ($A \approx 2.0$).

To separate the properly identified protons, gates have been applied to the two types of mass spectra. However, to demonstrate the experimental signature of events lacking full energy deposition, these gates have been opened wide creating the spectra in Figs. 2(b) and 3(b). These data also require a coincident proton in one of the two opposite detectors with energies that kinematically select the 2NA process. The dashed lines in Figs. 2(b) and 3(b) show the equivalent Monte Carlo (MC) generated data (see Sec. II C), demonstrating the success of the simulation of the experimental imperfections discussed. The gates actually used in the analysis are indicated by arrows in Figs. 2 and 3. Note that these gates are liberal to minimize any possibility of cutting off the cross section in an uncontrolled fashion. Consequently, a certain number of not fully stopped protons in the low mass tails are accepted both in the experimental and in the MC generated data.

The full thickness of the ΔE-E telescopes of 19 cm is sufficient to stop protons of up to 179 MeV at normal incidence and of slightly higher energy at out-of-plane angles. Thus, nearly all protons from two-nucleon absorption at 114 MeV pion energy are stopped, but not at 162 MeV. At the higher pion energy, a large number of such protons penetrate the most forward telescopes (1, 2, 14, 15) depositing only a fraction of their energy in the detectors. An algorithm was developed to determine the total energy from the detected energy fraction. The results have been used to recheck the energy calibrations at 162 MeV and to calibrate the energy loss tables used in the Monte Carlo simulations (Sec. II C). In the remaining analyses of the data for this paper this conversion from detected energy fraction to total kinetic energy has not been used. Rather, the majority of the punch-through data have been excluded from the spectra via the particle identification gates (Figs. 2 and 3), for both the experimental and the MC generated data.

Time-dependent gain stabilization algorithms using self-consistency tests kept the absolute energy calibration stable to within $\approx 1\%$ and the TOF calibration accurate to within less than 100 ps. Figure 5 shows an example of how the TOF calibration changes with the time of day; it demonstrates the need for a sophisticated run-time dependent calibration to obtain the time and position resolution achieved. The changes visible are nearly 2 ns which is very significant considering flight times as short as 5 ns. The main reason for these fluctuations was insufficient air conditioning of the electronics modules.

The TOF resolution of 530 ps is dominated by the uncertainty of the start time from the beam telescope. The vertical position resolution on the ΔE detectors, derived from the TOF difference between the ends of each detector, is 22 mm as determined from calibration runs with apertures on the detectors. The angular uncertainty of 12° to 21° is dominated by the width of the detectors. The energy resolution at 253 MeV of total energy (absorption on deuterium) is 19 MeV. The average experimental uncertainty in the missing momentum determina-

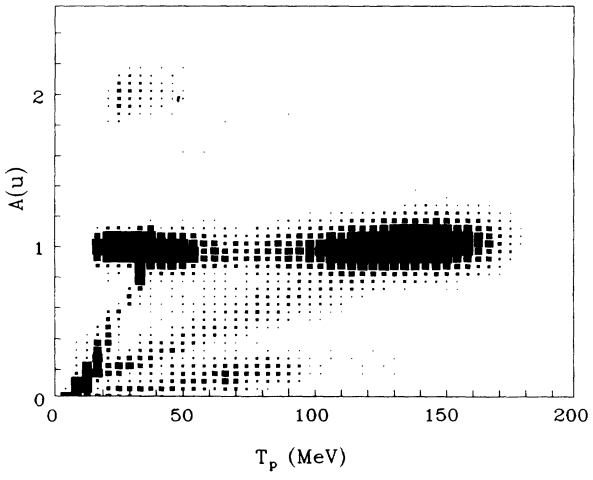

FIG. 4. The number of counts detected after the absorption of 114 MeV pions is shown, proportional to the size of the symbols, as a function of the kinetic energy and the mass of the particles. The mass identification uses the TOF-energy method. The energy is derived from the light in the scintillation detectors and is corrected event by event for all energy losses in nondetector material. Data for telescope 3 are shown with no gates applied. A projection of these data on the vertical axis results in Fig. 2(a).

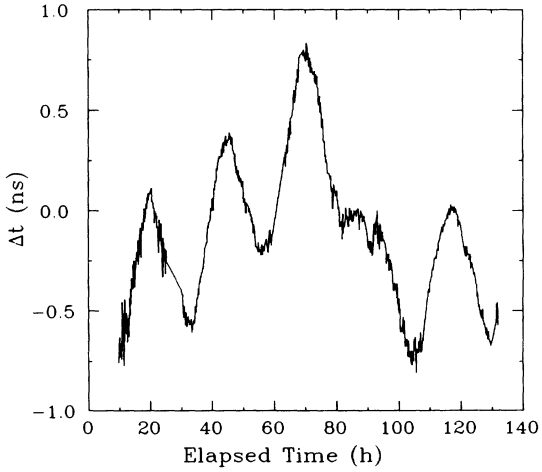

FIG. 5. The amount of time correction, Δt, applied to the average TOF measurement as a function of elapsed time in 6 minutes intervals, that is necessary for the TOF determination of particles recorded in detector $\Delta E-8$. In the 140-hour period covered by the horizontal scale, the electronic TOF determination drifted by more than 1 ns. The daily period of 24 hours is easily visible in the oscillations of the distribution.

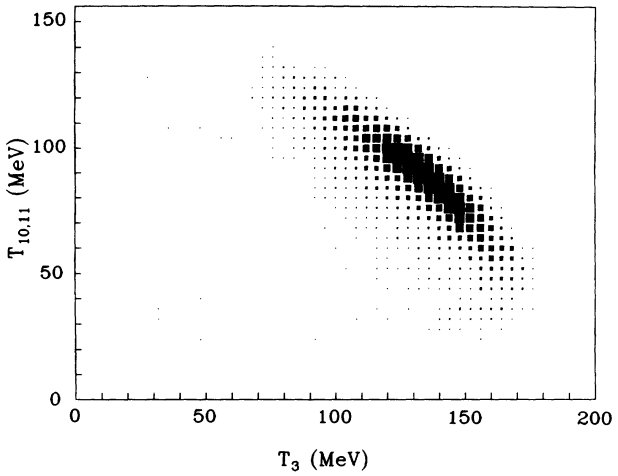

FIG. 6. The number of counts for two-proton coincidence events detected after the absorption of 114 MeV pions is shown proportional to the size of the symbols as a function of the kinetic energies of the two protons. The first proton is detected in telescope 3, the second one in telescope 10 or 11.

tion is about 75 MeV/c. All resolution values represent the full width at half maximum, FWHM.

A two-dimensional spectrum representative of events from the 2NA process is shown in Fig. 6. The gates require two protons to be detected in two telescopes separated by approximately 180°. The expected strong negative correlation in the energies of the two protons is visible in the long diagonal peak. The curvature of this peak is a consequence of the changing amount of residual nucleus recoil energy, which is largest in the wings of the distribution.

C. Monte Carlo simulation

A Monte Carlo (MC) simulation of the experimental apparatus was performed using a modified version of the code GEANT/GHEISHA [27] to create and track events which simulated the experiment as closely as feasible. The code had to be modified to accurately reproduce nuclear reactions and energy losses down to the lowest particle energies of this experiment. All details of the geometry of the experimental setup, including the various energy absorbing dead layers, were defined in the code and each individual fragment was tracked in 1 mm steps. The GEANT range calculations agreed within 1% with the experimental results (Sec. II B). Nuclear reactions of the fragments in the detector material were taken into account by providing appropriate cross-section tables [28]. The energy losses were converted to their light equivalent. Light, TOF, and position information were modified randomly according to the experimental resolution functions. Final results were recorded event by event in the same format, and later analyzed in the same way, as the calibrated experimental data.

The type of event generator used for the MC simulation depended on the reaction process. In the QDA model of two-nucleon absorption (2NA) the ^{4}He nucleus ejects two energetic protons while the residual deuteron (d) recoils with momentum k_d. In the first step of the QDA simulation, the (π^+ + ^{4}He) system disintegrates randomly into a deuteron and two protons with a phase-space probability distribution. In the second step, the deuteron momentum distribution is folded with the Fermi momentum density distribution, ρ, of the spectator deuteron given by

$$\rho(k_d) \propto \exp[-0.5(k_d/k_F)^2] \quad (1)$$

with the Fermi momentum parameter k_F adjusted to reproduce the experimental data. The best value of k_F=89 MeV/c, obtained for both sets of data (114 and 162 MeV), is in good agreement with ^{4}He($e,e'd$) quasielastic electron scattering data [29]. The data are compatible with changes in k_F of about ±6 MeV/c. Due to the large coverage of phase space the uncertainty in k_F results in a much smaller corresponding uncertainty in the extracted cross section of less than 1.4% which is included in the systematic uncertainty. The first two steps of the simulation provide a phase-space calculation in a spectator model. In a third step the probability of each event is further modulated with the ^{2}H(π^+,pp) cross section [2] as contained in a plane-wave impulse approximation (PWIA) treatment of the QDA [30] (see Sec. II E).

Calculations for pion absorption on clusters of four nucleons (4NA) and on three nucleons with a spectator nucleon (3NA) were done using the first step with a phase space distribution for four independent nucleons. For 3NA the second step was needed also, with a momentum distribution appropriate for a single nucleon in ^{4}He (k_F = 76 MeV/c).

Absorption on a T = 1 pn pair (non-QDA 2NA) should have practically the same angular correlations as QDA since these primarily reflect the momentum distribution of the spectator nucleus. It is likely that the angular distribution for T = 1 absorption is also very similar to that of QDA [5, 19]. The forward-backward asymmetry observed in pn final states has to disappear for a pp final state. Thus, the QDA-MC simulation should also reasonably represent 2NA on a T = 1 pn pair.

D. Cross-section determination

The cross sections presented in this paper have been obtained by a comparison of the experimental data with the MC simulation data. For this purpose, both the experimental and the MC-generated data have been analyzed in an identical manner. Most importantly, identical gating conditions on particle identification, energies, angles, etc. were used. The ratio of the total number of MC events generated to the number detected is the extrapolation factor, which accounts for solid angle limitations, particle misidentifications, threshold and resolution effects, etc.

The total cross section is obtained from the total number of experimental counts within the gates multiplied by the MC extrapolation factor for these gating conditions and normalized to the incident pion flux and target

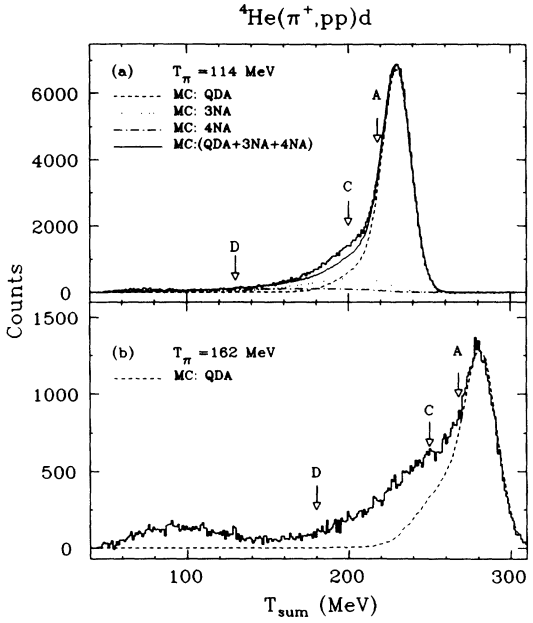

FIG. 7. Energy spectra for the sum of the kinetic energies, $T_{\rm sum}$, of two detected protons plus the calculated recoil energy for the absorption of (a) 114 MeV and (b) 162 MeV pions in ^{4}He. The dashed lines represent the MC simulation for PWIA-QDA. In (a) the dotted and dash-dotted lines are MC simulations for three-, 3NA, and four-nucleon absorption, 4NA, respectively. The solid line is the sum of MC simulations for QDA, 3NA, and 4NA. All MC curves are smoothed and normalized to be compatible with the data. The arrows indicate the limits used in the tables. The limit given by arrow A at $E_{\rm miss}$ = 12 MeV is also used in the creation of the subsequent figures. The $E_{\rm miss}$ scale has its origin at the center of each peak and increases towards smaller $T_{\rm sum}$ values.

thickness. For the differential cross sections in the angular distribution the appropriate extrapolation factor at each point is the ratio of all MC events generated within the solid angle for one of the protons to MC events detected with all gates applied.

Given a good model for the MC simulation, this method makes the cross-section determination independent of any specific selection of the data used. This means that using a single point of the total energy distribution in Fig. 7 gives, in principle, the same result as using a wide range of the distribution. This property allows us easily to exclude regions of the data that are contaminated by non-2NA processes without influencing the result, if the model is perfect. In general, it can be expected that the smaller the extrapolation factors are, the smaller is the dependence of the result on the quality of the model. Using the MC simulation to extract cross sections also automatically eliminates any double counting problems.

E. PWIA and DWIA calculations

The MC simulation for QDA (Sec. II C) contains the deuteron absorption cross section in the PWIA approximation. For this purpose, the relative motion of the pion and the absorbing deuteron cluster is transformed into their instantaneous center-of-mass system and the ^{2}H(π^+, pp) cross section is evaluated at the pion energy in this reference frame. The method used, which neglects any binding energy effects, corresponds to the initial energy prescription (IEP) of Ref. [30]. An alternative method is the final energy prescription (FEP) which reduces the pion's kinetic energy to account for the binding energies of the emitted nucleons. The IEP appears to reproduce the data best [7].

Several calculations have been performed with the distorted wave impulse approximation (DWIA) program THREEDEE [30]. These DWIA calculations used optical model parameters from Ref. [31] and a bound deuteron wave function adjusted to reproduce the experimental momentum distribution. For additional information about THREEDEE see Refs. [10–13].

The DWIA results have been used for two purposes. First, it is important to obtain an estimate on how much the DWIA angular, energy, and momentum distributions deviate from the PWIA results. It was found that for the reaction under study the differences are very small in contrast to results obtained for heavier nuclei [10–13].

Secondly, the DWIA allows us to obtain an estimate for the probability that a final-state proton undergoes a final-state interaction (FSI) in a second step after the primary "pure" 2NA process. This information is obtained by comparing the cross sections using the full DWIA calculations, with all optical potentials present, with calculations where the imaginary part of the optical potential in the exit channel is set to zero. This method has been used successfully in the interpretation of previous experiments [7, 10–13]. The results indicate that in about 30% of the events at least one of the protons should undergo a FSI with the spectator deuteron. Among the processes contributing to FSI are inelastic excitation of the spectator nucleus, quasifree knockout of a nucleon ("hard" FSI), or pickup of a nucleon ("soft" FSI).

III. RESULTS

A. Summed energy spectrum

For a reaction leading to a three-body final state, like a one-step QDA on ^{4}He resulting in a *ppd* final state, the detection of the momenta and masses of two particles is sufficient to unambiguously (within the experimental resolution) determine the kinematics of all three particles. Energy conservation requires that the sum of the kinetic energies of the three particles $T_{\rm sum}$ (i.e., the measured kinetic energy of two detected protons and the calculated kinetic energy of the undetected deuteron, thus assuming a three-body final state) has to be a constant value, $E_{\rm tot}$, if no excitation energy is involved, $T_{\rm sum} = E_{\rm tot}$. In contrast, a four-body breakup of ^{4}He does not allow for such a calculation from the measurement of two particles only; an attempt will result in an energy sum in which energy is apparently missing, $E_{\rm miss} = E_{\rm tot} - T_{\rm sum}$.

The shape of the $T_{\rm sum}$ spectrum can give important information about the final-state products and thus also

about the reaction mechanisms involved. The $T_{\rm sum}$ spectrum is better suited for this purpose as compared to the simple sum of the two proton energies since the kinetic energies for the "recoiling" deuterium nucleus can be substantial due to its small mass as is evident from the curvature of the peak in Fig. 6. A spectrum of the sum of just the two proton energies has a significantly increased width for the main peak, and thus worse resolution than the $T_{\rm sum}$ spectrum in Fig. 7.

In principle, 2NA can lead directly to excited states of the recoil nucleus in addition to the ground state (see, e.g., [7, 10]). For the closed shell ^{4}He target nucleus, however, one can expect only very small overlap of the ^{4}He ground-state wave function with any excited states in deuterium, and thus low cross sections. The only exception is the $T = 1$, $S = 0$ first excited state near 2 MeV of excitation energy; 2NA to this state is not QDA (T=0 np pair) since the pion is absorbed on a T=1 np pair. This excited state is not resolved in the present experiment and will contribute to the extracted 2NA cross section. Absorption on a T=1 nucleon pair is about a factor of 20 smaller than QDA [5, 19, 23]. Thus we can expect that essentially all the pure one-step 2NA cross section is found within a few MeV of the ground state and that our 2NA results are dominated by QDA.

Figure 7(a) shows the $T_{\rm sum}$ spectrum for the 114 MeV data. A pronounced Gaussian shaped peak is located at the expected energy of $T_{\rm sum}$ = 230 MeV ($E_{\rm miss}$ = 0 MeV) with a low-energy tail, corresponding to higher $E_{\rm miss}$. The MC simulation for QDA (dashed line) reproduces this peak and a small part of the tail. This MC-predicted tail originates from incomplete kinetic energy detection for protons undergoing nuclear reactions or for protons not being fully stopped in the detectors (Sec. II B). These effects have been carefully modeled and extensively tested in the MC simulations (Figs. 2 and 3). While many of such events are rejected by the analysis procedure, resulting in the disappearance of the MC tail near $E_{\rm miss}$ = 50 MeV, the events in the remaining MC tail did satisfy our analysis criteria.

The excess yield in the experimental tail above the MC prediction cannot originate from a three-body ppd final state and thus cannot be part of the pure one-step 2NA cross section. To explore the possible origins of the excess yield in the experimental tail of the 114 MeV data, MC simulations for 3NA and for 4NA have been performed with the absorbing nucleons uniformly populating phase space. An analysis of these 3NA and 4NA data with a procedure identical to the QDA analysis shows that the calculated summed energies fall into the region of the tail (dash-dotted and dotted lines, respectively, in all figures). However, after normalization of 3NA and 4NA to the low-energy region (high $E_{\rm miss}$) in Fig. 7, we find that these two processes together cannot fully account for the excess yield in the tail. The origin of this tail will be further discussed in Sec. III E. From Fig. 7(a) it is apparent that a small part of 3NA and 4NA may also contribute to the main peak.

Figure 7(b) shows the summed energy spectrum for the 162 MeV data. Here only the QDA-MC simulation curve is shown. At this energy the low $E_{\rm miss}$ tail is stronger than at 114 MeV. This is mostly the result of the significant fraction of the 2NA reaction products at forward angles that penetrates the 19 cm of detector material (see Sec. II B). This increases the tail yield and at the same time reduces the yield in the peak proper. (However, most of the punch-through protons are not visible since they are rejected by the analysis procedure.) In contrast, in the 114 MeV reaction essentially all of these protons are stopped in 19 cm of detector material. The MC simulation is in agreement with these differences between the 114 and 162 MeV data as is visible from the dashed curves. It can be seen that also at 162 MeV there is significant yield in the tail beyond the QDA-MC prediction.

At both energies a small broad peak is visible at very low $T_{\rm sum}$ which is not predicted by any of the MC calculations performed. These events are not due to an experimental artifact such as misidentified particle type or energy, they are due to proton pairs with low kinetic energies for each proton, mainly at off-quasifree angle pairs. The dynamic process leading to these events has not yet been identified.

B. Missing momentum spectrum

From Fig. 7 it is obvious that only part of the energy range can be used if one wants to explore pure 2NA. A detailed investigation has shown that for $E_{\rm miss}$ below about 12 MeV (i.e., above the arrow A in Fig. 7) the total cross section extracted via extrapolation with the MC simulation does not depend on the $E_{\rm miss}$ data region chosen. In contrast, in the tail region with $E_{\rm miss} \geq 12$ MeV the extrapolated cross section changes as a function of $E_{\rm miss}$ cut due to the presence of processes other than pure 2NA. Thus the data in the peak of Fig. 7 below 12 MeV of $E_{\rm miss}$ can be used to investigate the properties of 2NA. However, this energy region of the peak may also contain events with a ppd final state not originating from 2NA, as well as some amount of four-body final states, like 3NA and 4NA [dotted and dash-dotted MC simulation lines in Fig. 7(a)].

The missing momentum $k_{\rm miss}$ can be calculated from the momenta of the pion in the beam and those of the two detected protons,

$$k_{\rm miss} = | \mathbf{k}_\pi - \mathbf{k}_{p1} - \mathbf{k}_{p2} |. \quad (2)$$

In Figs. 8(a) and 8(b) the missing momentum spectra for all events with less than 12 MeV $E_{\rm miss}$ are shown. The expected distribution of counts for a 2NA reaction proportional to $k^2_{\rm miss}\rho(k_{\rm miss})$ [with $\rho(k_{\rm miss})$ being the momentum density distribution of the undetected recoil deuteron, see Eq. (1)] is modulated due to the granularity of the detector system. The QDA-MC simulation (dashed line) reproduces the main features of the distribution very well up to about 250 MeV/c.

At higher $k_{\rm miss}$, the experimental data show a substantially higher yield than the MC simulation. Part of the excess yield may be due to distortion effects in the QDA not incorporated in the PWIA-MC calculations. The excess yield may also reflect a spectator deuterium recoil momentum distribution that is not purely Gaussian but

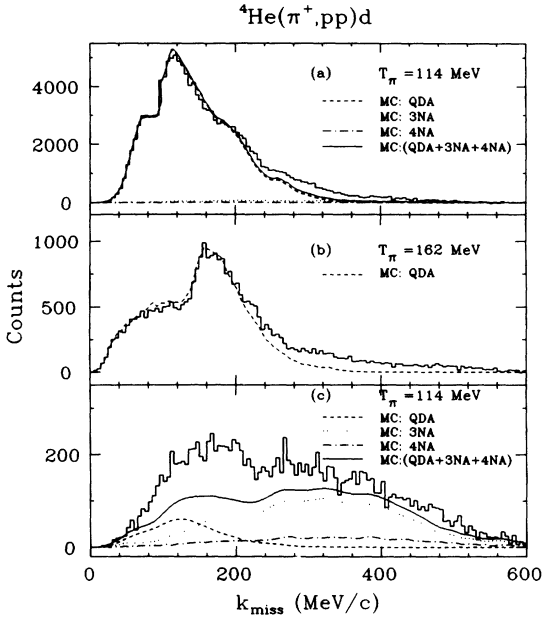

FIG. 8. (a) The missing momentum distribution k_{miss} for all data in Fig. 7(a) with missing energies E_{miss} below 12 MeV. The curves for the MC simulations are the same as in Fig. 7(a) with the same relative normalizations. The oscillations with a period of about 50 MeV/c superimposed on the main peak are an experimental artifact originating from the discreteness of the 16 detector telescope setup. (b) The equivalent data for 162 MeV pion absorption. Only QDA-MC simulations are shown as the dashed curve. (c) is similar to (a), however, with an E_{miss} cut from 30 to 50 MeV [region near arrow C in Fig. 7(a)].

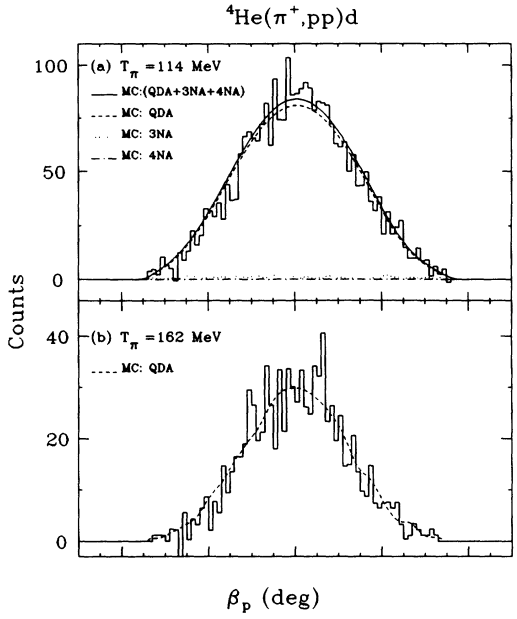

FIG. 9. Out-of-plane angular correlation between two protons from (a) 114 MeV and (b) 162 MeV pion absorption in ^{4}He. Only events with E_{miss} below 12 MeV and k_{miss} below 250 MeV/c are accepted. One proton is detected at an in-plane angle of $\theta = 64.3° \pm 8.0°$ with an out-of-plane acceptance of $\beta = \pm 8.9°$ in telescope 4. The other proton is detected in telescopes 11 or 12 with a θ range of $-75°$ to $-111°$ (the out-of-plane distribution being shown). The fitted FWHM of $32.5° \pm 0.8°$ is reduced to an intrinsic width of 29.4° for the out-of-plane angular correlation after unfolding other contributions. The MC simulation curves are the same as in Fig. 8 with the same relative normalizations.

contains significant amounts of high momentum components. Unfortunately, the data in Ref. [29] only extend to about 250 MeV/c and thus do not answer this question. In both these cases, the excess yield would be part of the 2NA cross section under investigation. In addition, it is possible that non-2NA processes contribute in this region in spite of the restrictive energy gate. Phase-space-like 3NA and 4NA cannot explain the yield as is evident from the corresponding lines in Fig. 8(a). However, significant yield could originate from 3NA or 4NA processes which are followed by a recombination of a proton and a neutron in a "soft" final-state interaction or from other processes with the same *ppd* final state as direct 2NA. This facet of the data is further discussed in Sec. III F.

The k_{miss} region below 250 MeV/c appears to be largely free of non-2NA events. Thus these data have been chosen, in conjunction with the extrapolations provided by the MC simulations, to produce the angular correlations and distributions discussed in the next two sections.

C. Angular correlation

Figures 9(a) and 9(b) show the out-of-plane angular correlation for proton-proton coincidences with the first proton defining the scattering plane and detected at a fixed angle of about +64° (telescope 4 in Fig. 1) and the second proton detected at an in-plane angle near −90° (telescopes 11 and 12). The FWHM of 29.4° (corrected for all experimental angular resolution effects) of the 114 MeV distribution in Fig. 9(a) is wide compared to ~ 15° for absorption on a *p*-shell *np* pair in ^{6}Li [7], but similar to absorption on an *s*-shell pair in ^{6}Li [7], a reflection of the tightly bound nature of the deuteron in the ^{4}He nucleus. Figure 9 demonstrates that our experimental setup samples the angular correlation far into the wings of the distribution [in Figs. 9(a) and 9(b) more than 99% of the Gaussian distribution area is within the limits of the data]. From the dotted and dash-dotted lines in Fig. 9(a) it is evident that phase-space-like 3NA and 4NA can only contribute insignificantly to the spectrum in Fig. 9(a). Even though these experimental data are taken at angles near the minimum of the QDA angular distribution, the yield is dominated by 2NA processes under the energy and momentum conditions applied.

The excellent agreement between the data and the QDA-PWIA-MC simulation (dashed line) verifies the accuracy of the simulation and emphasizes the dominance of QDA-like events in the data region selected. Even though the PWIA-MC calculations do not take distortions into account, this comparison, as well as our DWIA

calculations (Sec. II E), indicate that the shapes of the angular correlations and distributions are not significantly affected by distortions in this reaction.

D. Angular distribution of cross section

The $T_{\rm sum}$ and $k_{\rm miss}$ distributions shown in Figs. 7, 8(a), and 8(b), as well as the angular correlations of Fig. 9, indicate that for $E_{\rm miss}$ below 12 MeV and $k_{\rm miss}$ below about 250 MeV/c the experimental data are compatible with the dominance of pure 2NA or even pure QDA as predicted by the MC simulations, whereas at higher $E_{\rm miss}$ and $k_{\rm miss}$ other processes might interfere. Thus, only these data are used to extract the angular distribution of the 2NA cross sections (Sec. II D). In addition, the out-of-plane position of the first proton (for which the angular distribution is determined) has been restricted to an out-of-plane range of ± 100 mm ($\pm 8°$ to $\pm 12°$) from the horizontal detector symmetry plane assuring that practically the whole out-of-plane range of the second proton is directly measured (Fig. 9). The nominal laboratory angle of the detector is taken as the scattering angle. The results of symmetric detector pairs (Fig. 1) are consistent with each other and have been averaged.

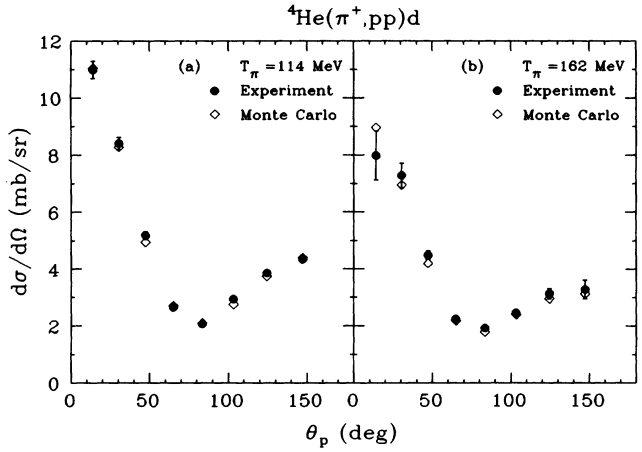

FIG. 10. Angular distribution of differential cross section in the laboratory system for one of the protons detected in two-proton coincidences from (a) 114 MeV and (b) 162 MeV pion absorption in ^{4}He. Only data within ± 100 mm (about $\pm 10°$) of the reaction plane, with $E_{\rm miss}$ below 12 MeV, and $k_{\rm miss}$ below 250 MeV/c are used. The interpolations between detectors and extrapolations into unmeasured regions of phase space are done by comparison with QDA-MC simulations. Experimental data are shown as filled circles and the QDA-PWIA-MC simulation as open diamonds. The error bars on the experimental data represent only the statistical uncertainties (counts and gate limits) originating from the experimental as well as the MC data. Statistical errors for the MC points are smaller than the symbols and have been omitted. The data points are placed at the nominal detector angles and represent values averaged over the θ_p range given approximately by the angular distance between the data points.

Figure 10 shows the resulting angular distributions of the measured (filled circles) cross sections in the laboratory system for one of the QDA protons after integrating over all degrees of freedom for the second proton. The dominant contribution to the extrapolations is from the in-plane gaps between the detectors. The resulting angular distributions are very similar to the ones of the ^{2}H(π^+, pp) reaction at the same pion energies. The forward peaking of the distribution is expected in the laboratory frame. The MC simulation provides the appropriate quantitative comparison of ^{2}H(π^+, pp) with the experimental data, since the MC includes the averaging effects of the large detector solid angles and of the dynamics of the QDA process via the PWIA. The cross sections from the MC simulation of QDA are shown in Fig. 10 as open diamonds, and are seen to provide an excellent representation of the data over the full angular range for the 114 MeV data [Fig. 10(a)]. Deviations between experimental and MC angular distributions could have been expected if distortion effects modify the angular distributions or if yields from non-QDA processes with different angular distributions are important. At 162 MeV [Fig. 10(b)] punch-through (Sec. II B) affects the most forward and most backward angle data. The increased error bars reflect the associated uncertainties.

An integration of the experimental angular distributions in Fig. 10, using a polynomial fit, yields cross sections that agree within the error bars to those extracted for cases A in Tables I and II.

Taking all the evidence discussed so far, we find that all data near $E_{\rm miss}=0$ and with $k_{\rm miss} \leq 250$ MeV/c are fully compatible with the properties expected for QDA. It is expected that about 5% of the cross section originates from 2NA on a $T=1$ 2NA [19] which apparently does not modify these QDA properties visibly.

E. The excess experimental yield in the low $E_{\rm miss}$ region

The MC simulations for QDA, 3NA, and 4NA cannot account for all of the cross section in the tail region of the main peak in Fig. 7(a). Excess yield is visible between about 20 and 60 MeV of $E_{\rm miss}$. While the yield may be due to non-phase-space-like 3NA or 4NA, different reaction channels may be present. Thus the data with $E_{\rm miss}$ between 30 and 50 MeV have been analyzed to explore the possible origin of this excess yield. The particle identification gates have been tightened for this analysis to suppress more strongly the yield from poorly identified particles (i.e., for instance, the QDA-MC yield in this region).

The experimental results for the missing momentum distribution are shown in Fig. 8(c). Also given in this figure are the MC simulation results for QDA, 3NA, and 4NA with the normalizations used for Fig. 7(a). As in Fig. 7(a), only part of the yield is accounted for by the MC data. However, this distribution gives some clear signatures for the excess cross section. The high momentum region is nearly quantitatively reproduced by the 3NA and 4NA simulations which peak at relatively high $k_{\rm miss}$. In contrast, only a small fraction of the low $k_{\rm miss}$

TABLE I. Cross sections are listed for the ^{4}He$(\pi^+,pp)d$ reaction at T_π=114 MeV using different selections of the experimental data (with at least two protons detected) and extrapolations based on QDA-model Monte Carlo calculations. The data regions used and the factors for extrapolations into excluded or unmeasured regions of phase space (as determined by the MC calculations) are given. k_{miss} is the missing momentum and E_{miss} is the missing energy calculated assuming a three-body final state. Case A can be taken as the pure 2NA cross section for the ^{4}He$(\pi^+,pp)^2$H reaction. The overall normalization uncertainty (systematic error) is estimated to be 7.0%. Relative uncertainties between cases are $\leq$2%. Also given are the ^{2}H(π^+,pp) cross sections [2] at the nominal beam energy (IEP) and at the beam energy reduced by the deuteron binding energy in ^{4}He (FEP). The results, after multiplication with a FSI correction factor of 1.41, can be compared with the total σ_{abs} = 68±15 mb.

"Case"	Data regions used		Extrapolation factor	Extrapolated 2NA-σ (mb)
	E_{miss} (MeV)	k_{miss} (MeV/c)		
A	< 12	< 250	5.74	25.74
B	< 12	< ∞	5.43	30.26
C	< 30	< ∞	4.63	32.77
D	< 100	< ∞	4.43	38.55
E	< 12	< 200	6.47	24.88
F	< 30	< 200	5.51	25.85
^{2}H(π^+,pp) at 114 MeV (IEP)				11.67
^{2}H(π^+,pp) at 90 MeV (FEP)				9.59

cross section is predicted by the QDA-MC simulation and only about half of it by the sum of all simulations. The excess yield above that predicted by MC [counts above the solid curve of Fig. 8(c)] has a distribution similar to that of Fig. 8(a), a strong suggestion that a large part of these events are closely connected to QDA. Indeed, the angular distribution of the experimental data in Fig. 8(c) has the same strong angular dependence as observed for 2NA.

These observations suggest that a considerable fraction of these events are related to the 2NA channels, while the final state cannot contain an intact recoiling deuterium due to the amount of missing energy. While a small fraction of 2NA might involve the excitation of the spectator deuteron to about 40 MeV, the most simple explanation is that these events originate from a two-step process in which 2NA is combined with a FSI or initial state interaction (ISI) which breaks up the spectator deuteron. Our DWIA calculations (Sec. II E) indicate that there is a considerable probability for FSI. Thus it is very likely that a substantial part of the events in the tail region originates from 2NA with subsequent FSI. The next section will provide a quantitative comparison. Apart from sequential FSI it is also possible that more complex processes not involving 2NA have angular distributions similar to that of QDA and give a significant contribution to these yields.

F. Tables of cross sections

Tables I and II contain the integrated cross sections for 2NA at 114 and 162 MeV, respectively, extracted from the experimental data using the QDA-PWIA-MC simulation for interpolation and extrapolation into the unmeasured regions of phase space (see Sec. II D) based on different selections of the data (cases A through F). The uncertainties of $\leq$2.0% between values in each table are dominated by uncertainties in the energy calibra-

TABLE II. Cross sections for the ^{4}He$(\pi^+,pp)d$ reaction at T_π=162 MeV. The FSI correction factor is 1.45 and σ_{abs} = 63±15 mb at this energy. Further details are described in the caption of Table I.

"Case"	Data regions used		Extrapolation factor	Extrapolated 2NA-σ (mb)
	E_{miss} (MeV)	k_{miss} (MeV/c)		
A	< 12	< 250	11.70	20.97
B	< 12	< ∞	10.95	27.33
C	< 30	< ∞	8.46	30.04
D	< 100	< ∞	7.56	42.64
E	< 12	< 200	13.91	20.13
F	< 30	< 200	10.52	20.95
^{2}H(π^+,pp) at 162 MeV (IEP)				10.99
^{2}H(π^+,pp) at 138 MeV (FEP)				12.28

tions; the combined statistical errors from the experimental and MC data are $\leq 0.5\%$. The relative uncertainty between Tables I and II, estimated to be less than $\pm 4\%$, is mainly due to uncertainties involving punch-through protons. An overall normalization uncertainty of $\pm 7\%$ due to systematic errors in target thickness, incident beam flux, corrections for nuclear reactions in detectors, uncertainty of the deuteron momentum distribution in ^{4}He, and geometry of the experimental setup has to be applied to the absolute values. As an independent confirmation of the absolute normalization, the (low statistics) $^4\mathrm{He}(\pi^+,\pi^{+'})$ elastic scattering data from this experiment have also been extracted by using an elastic scattering Monte Carlo simulation of this process. The results are 7% higher than cross sections from an interpolation of recent 110 and 130 MeV data [32] (which have a systematic uncertainty of about 7%).

Also given in Tables I and II are the extrapolation factors which represent the ratio of total MC events generated to events accepted by the data analysis procedure. These factors are 5.7 at 114 MeV and 11.7 at 162 MeV for case A. The value for 162 MeV is larger due to fewer protons being fully stopped by the detectors, which reduces the acceptance. These factors have to be compared with extrapolation factors in previous experiments which are orders of magnitude larger, reflecting mainly the differences in solid angle coverage. In fact, the present experiment samples a much larger fraction (about 68%) of all possible different phase space elements than the extrapolation factors indicate (although with less than 100% efficiency) since all angles around the beam axis are equivalent. About half of the remaining angle combinations give negligible contributions to QDA.

In the determination of the cross sections in Tables I and II possible contributions from 3NA and 4NA have been ignored. For cases A, B, and E ($E_{\mathrm{miss}} \leq 12$ MeV) in the tables such contaminations should be very small as indicated by the MC simulation in Fig. 7(a). A *ppd* final state with a deuteron that is not just a spectator should have mostly larger k_{miss} than accepted in cases A, E, and F. It cannot be completely excluded that a non-2NA process with an unexpected distribution in phase space might peak in the acceptance of these gates, such that even a low cross-section process yields some contribution. However, overall, the restrictive gates and the shape of the angular correlations and distributions make it very likely that any such contributions are very small and that 2NA dominates for cases A and E.

Note that all cross sections inherently assume QDA kinematics via the MC simulation. This is appropriate also for 2NA on a $T=1$ *np* pair (Sec. II C), but any additional cross section extracted which originates from processes other than 2NA can only be used for qualitative comparisons.

The cleanest representation of the 2NA cross section is provided by the experimental data with E_{miss} below about 12 MeV (see Fig. 7) and k_{miss} below 250 MeV/c (see Fig. 8), i.e., case A in Tables I and II. The properties of the data within the gates of case A are, in general, in very good agreement with the QDA-MC simulation results as can be seen in Figs. 7–9. Comparing the resulting experimental yields with those obtained from a QDA-MC simulation analysis under identical conditions results in a 2NA cross section of 25.7 mb at 114 MeV and 21.0 mb at 162 MeV. This is the 2NA cross section where the deuteron is left as a spectator in (or near) its ground state and recoils according to its Fermi momentum distribution. The major part of this 2NA cross section should be QDA ($T=0$ *np* pairs) while 2NA on a $T=1$ *np* pair should only constitute a fraction of about 5% of the total (5% has been found for π^- absorption on *pp* pairs [5, 19]).

The same analysis without the restriction on k_{miss} (case B) results in an increased value for the cross section of 30.3 mb (27.3 mb) for the 114 (162) MeV data reflecting the excess of experimental over MC simulation data above 250 MeV/c of k_{miss} (Fig. 8). The additional cross section of 4.5 (6.4) mb, compared to case A, indicates the presence of significant yield for *ppd* events with high k_{miss} which have the same final state as QDA but which are not consistent with our PWIA-QDA model. As discussed in Sec. III B these events may indicate either the need for modifications of the QDA model or the presence of additional, more complicated reactions with the same final state as 2NA. If only the model is inadequate, then the case B cross section would be a close representation of the pure 2NA yield. In this situation one would expect that the fraction of cross section in the high momentum region is independent of beam energy. However, when comparing cases A and B, we find the additional "cross section" to be quite different, amounting to 18% and 28% of the case A values for 114 and 162 MeV, respectively. This makes it rather likely that additional, non-QDA processes with a different energy dependence dominate the high momentum region. For instance, calculations by Oset *et al.* [33] for ^{12}C predict a strong pion energy dependence for the 3NA process.

Relaxing the conditions on the data one step further by including 30 MeV of the low energy tail in Fig. 7 (case C) in the comparison of experimental and MC data, one obtains an additional 2.5 mb (2.7 mb), representing 10% (13%) at 114 MeV (162 MeV) of the pure 2NA cross section of case A. This region still excludes more than half of the 3NA and 4NA phase space [see Fig. 7(a)], but may contain a large fraction of 2NA+FSI events. An even stronger suppression of 3NA and 4NA phase space is obtained when comparing cases E and F, which exclude the high k_{miss} data; for this a 4% increase in cross section is found. It was observed previously in Sec. III E in the discussion of Fig. 8(c) that the excess counts in this region of the tail have properties very similar to those of QDA. However, they require a four-body final state which could originate from 2NA+FSI. The values for the increased cross section for $E_{\mathrm{miss}} \leq 30$ MeV (comparing cases B and C) of 10 to 13% can easily be accommodated by a correction factor of 1.4 (=40%) for FSI predicted by our DWIA calculations (Sec. II E). The fraction of events experiencing FSI increases slightly with energy based on our DWIA calculations (29% at 114 MeV compared to 31% at 162 MeV). This is compatible with the experimental observations. The combined evidence suggests that a considerable fraction of events undergoing FSI can

experimentally be found in the low $E_{\rm miss}$ tail region of the peak in Fig. 7 (the remainder would be expected in other regions of the four-body phase space). Any 2NA that goes directly to unbound excited states of the residual deuterium would contribute to this $E_{\rm miss}$ region as well.

For the cases without restriction on $k_{\rm miss}$ (cases B, C, D), a substantial amount (20–50 % of the additional data) is experimentally accompanied by a third observed particle (a proton, neutron, or deuteron). While some of these are recoiling deuterons with energies above our detector threshold of about 24 MeV or 300 MeV/c, the remaining events give direct evidence for the existence of a non-2NA process with a *ppd* final state. Events with a third proton or neutron are to be expected for 3NA or 4NA as well as for 2NA accompanied by ISI or FSI. Such events demonstrate the existence of processes other than pure 2NA in the high momentum region of Fig. 8.

Cases D and E in Tables I and II explore further the limits that one might impose on the accepted data. If there exist any reactions other than 2NA then at least part of their yield can be expected to be included in the limits of case D. From our data we do expect about 50% of the total absorption cross section to be found in other channels (see below). However, any distribution in space different from the one used in the QDA model will make the additional computed "cross section" values meaningless. Case E is more restrictive on the recoil momenta accepted than the "ideal" case A. Even though we consider any data below 250 MeV/c to be representative of 2NA, the result that the cross sections for case E are reduced by 3 to 4% as compared to case A is just a reflection of the observation that the MC curves in Figs. 8(a) and 8(b) are merely good representations of the experimental data, not perfect ones. This discussion of cases A through E also demonstrates the range of results one can obtain if the kinematics of the reaction is not sufficiently defined.

For comparison with Ref. [19], identical regions in energy and $k_{\rm miss}$ were applied to our 114 MeV data (case F in Table I). Under these conditions our data yield 25.9±1.8 mb for the 2NA cross section, which is 30% smaller than previously reported (36.9±8.9 mb) at the slightly higher beam energy of 120 MeV. Only about a 3% increase in cross section can be expected to be due to the higher energy. The remainder of this difference, as well as their large uncertainty of 24%, may be a consequence of the comparatively small solid angle coverage in Ref. [19] resulting in much larger extrapolations as compared to the present work. Also, due to its impact on the angular correlations, any uncertainty in the shape of the recoil momentum distribution [e.g., defined by k_F in Eq. (1)] can lead to large cross-section errors, if only part of the out-of-plane angular correlations are covered as is the case in Ref. [19].

IV. SUMMARY AND CONCLUSIONS

In summary, the current ^{4}He(π^+, pp) experiment directly identifies 25.7 mb (at 114 MeV) and 21.0 mb (at 162 MeV), with an overall systematic uncertainty of ±7% and a relative error of ±4%, of pure 2NA cross section which is substantially less than previously reported [19]. Approximately 95% of this should originate from QDA. These values require that the spectator deuteron is left near its ground state. These cross sections are 2.2 (1.9) times the ^{2}H(π^+, pp) cross sections, $\sigma_{^2\rm H}$ [2], at 114 (162) MeV and do not directly support the idea that two-nucleon pion absorption in ^{4}He can be accounted for by simple isospin counting of three proton-neutron pairs in ^{4}He with the deuterium quantum numbers [18]. Our DWIA calculations indicate that at 114 (162) MeV only 71 (69)% of the initial QDA events survive the reaction undisturbed by FSI. This provides an estimate for a primary QDA absorption cross section before FSI of 36.3 (30.4) mb or $3.1\sigma_{^2\rm H}$ ($2.8\sigma_{^2\rm H}$) at 114 (162) MeV. (Note that these values are close to the ones quoted in Ref. [19], although in that work no corrections for the "hard" FSI, discussed in the current paper, have been used.)

Even though finding about 3.0 times the deuterium absorption cross section in our reaction is very suggestive, considering the three quasideuterons in ^{4}He from isospin counting, the cross-section ratios are based on the (arbitrary) reference to the cross section of 114 (162) MeV pion absorption on real deuterium. This approximates the "initial energy prescription" (IEP) of Ref. [30]. Alternatively, one can use the "final energy prescription" (FEP), approximated by subtracting the reaction Q value from the incident pion energy, as a substitute for taking off-shell effects into account in the absorption process. The FEP would require using $\sigma_{^2\rm H}$ at 91 (141) MeV instead of the nominal value of 114 (162) MeV ($\sigma_{^2\rm H}$ are given in the tables). This results in the FSI corrected cross sections of $3.8\sigma_{^2\rm H}$ ($2.5\sigma_{^2\rm H}$), giving an excitation function of QDA in ^{4}He very different from the one in deuterium. In contrast, the IEP with $3.1\sigma_{^2\rm H}$ ($2.8\sigma_{^2\rm H}$) yields an excitation function much more similar to the one in deuterium. Thus, it is likely that off-shell effects are small or have a weak energy dependence.

These results do not indicate any drastic modifications of the 2NA cross section due to the higher density of ^{4}He as compared to deuterium. However, a direct cross section comparison does not take into account any ISI of the pions or attenuation of the pion flux through the nucleus due to shadowing by nucleons, which may counteract an intrinsically increased cross section per pn pair.

Combining the present results, corrected for FSI effects, with total absorption cross sections of 68 mb and 63 mb (± ≈15 mb) at 114 and 162 MeV, respectively, we find that about 53% and 48% of the total absorption cross section is due to 2NA on pn pairs in ^{4}He at these energies. (The total absorption cross sections have been extracted from the calculations of Thies [34, 35] which provide a good average representation of the experimental values [35].) We obtain similar results at both energies: about 50% of the absorption cross section is due to 2NA or QDA, about 35% is unmodified by two-step processes and is directly observed experimentally. These percentages weakly support the expectations that the non-2NA cross section increases with energy ([33], Sec. III F), which would imply that the 2NA cross section fraction decreases with energy. However, the large

uncertainties of the total absorption cross sections do not allow to draw any definite conclusions.

Our results for ^{4}He can be compared with results for 2NA on pn pairs in other nuclei. For ^{3}He about 70 to 80% of the π^+ absorption cross section has been identified as 2NA [5], the remainder as 3NA. This result is nearly independent of beam energy up to 165 MeV [5]. For ^{6}Li [7] and ^{16}O [11–13,26] the fraction of 2NA decreases from close to 100% at low pion energies to approximately 50% at 165 MeV. At 115 MeV the fraction is about 60% for ^{6}Li and about 75% for ^{16}O. Unfortunately, all these values for nuclei with $A>3$ suffer from the large uncertainties in the knowledge of the total absorption cross sections. However, the combination of all these results suggests that the addition of one nucleon in going from ^{3}He to ^{4}He increases the cross sections for absorption channels other than 2NA considerably. Surprisingly, adding even more nucleons (^{6}Li, ^{16}O) does not seem to increase the non-2NA fraction in the Δ resonance region. In fact, at low pion energies those channels might even be suppressed again. Clearly, it would be very desirable to also have reliable results for 2NA on ^{4}He at lower energies.

The large coverage of available phase space in this experiment allowed us to verify expectations about the shape of the angular distributions and correlations for the QDA process, the dominant contribution to the measured 2NA process. We find that they are reproduced nearly quantitatively by our QDA-PWIA-MC simulation. From this observation we conclude that the QDA model used is applicable to a high degree of accuracy and that distortion effects have very little impact on the distributions of the cross section for our reactions. However, the primary cross section is reduced significantly (about 30%) by exit channel distortions even for this light nucleus. We find evidence for some of this missing 2NA cross section in the tail region of Fig. 7(a) as postulated previously [7]. The present data are compatible with a certain amount of 3NA and 4NA cross section [Figs. 7(a), 8(a), 9(a)]. More complete multinucleon coincidence data have been taken in this experiment and are being analyzed. These will allow a more quantitative determination of the non-2NA channels which may contribute the remaining 50% of the absorption cross section in ^{4}He, much more than previously anticipated [19,20].

ACKNOWLEDGMENTS

We thank the staff at PSI for the excellent beam and the outstanding logistic support for this experiment. We thank Jan Visschers (NIKHEF-K) for his important contributions during the design stage of this experiment. Without Yan Lefevere's (NIKHEF-K) construction of the cryogenic target and his help with the detector setup the experiment would not have been possible. Special thanks also go to B. van den Brandt and J. A. Konter of the PSI Cryo Group for the help with the liquid He supply system. Finally, we would like to thank N. S. Chant for many fruitful discussions about the impulse approximation calculations. The experiment was supported in part by the U.S. National Science Foundation and the Department of Energy.

[1] H. J. Weyer, Phys. Rep. **195**, 295 (1990).

[2] B. G. Ritchie, G. S. Blanpied, R. S. Moore, B. M. Preedom, K. Gotow, R. C. Minehart, J. Boswell, G. Das, H. J. Ziock, N. S. Chant, P. G. Roos, W. J. Burger, S. Gilad, and R. P. Redwine, Phys. Rev. C **27**, 1685 (1983); B. G. Ritchie, *ibid.* **28**, 926 (1983), and references therein.

[3] K. A. Aniol, A. Altman, R. R. Johnson, H. W. Roser, R. Tacik, U. Wienands, D. Ashery, J. Alster, M. A. Moinester, E. Piasetzky, D. R. Gill, and J. Vincent, Phys. Rev. C **33**, 1714 (1986).

[4] G. Backenstoss, M. Izycki, P. Salvisberg, M. Steinacher, P. Weber, H. -J. Weyer, S. Cierjacks, S. Ljungfelt, H. Ullrich, M. Furić, and T. Petković, Phys. Rev. Lett. **55**, 2782 (1985).

[5] S. Mukhopadhyay, S. Levenson, R. E. Segel, G. Garino, D. Geesaman, J. P. Schiffer, G. Stephans, B. Zeidman, E. Ungricht, H. Jackson, R. Kowalczyk, D. Ashery, E. Piasetsky, M. Moinester, I. Navon, L. C. Smith, R. C. Minehard, G. S. Das, R. R. Whitney, R. McKeown, B. Anderson, R. Madey, and J. Watson, Phys. Rev. C **43**, 957 (1991), and references therein.

[6] P. Weber, G. Backenstoss, M. Izycki, R. J. Powers, P. Salvisberg, M. Steinacher, H. J. Weyer, S. Cierjacks, A. Hoffart, H. Ullrich, M. Furic, T. Petkovic, and N. Simicevic, Nucl. Phys. A**501**, 765 (1989); P. Weber, G. Backenstoss, M. Izycki, R. J. Powers, P. Salvisberg, M. Steinacher, H. J. Weyer, S. Cierjacks, A. Hoffart, B. Rzehorz, H. Ullrich, D. Bosnar, M. Furic, T. Petkovic, and N. Simicevic, PSI Report No. PSI-PR-91-03 (1991).

[7] D. Zhang, Ph.D. thesis, University of Maryland, Maryland, 1990.

[8] R. D. Ransome, V. R. Cupps, S. Dawson, R. W. Fergerson, A. Green, C. L. Morris, J. A. McGill, J. R. Comfort, B. G. Ritchie, J. Tinsley, J. D. Zumbro, R. A. Loveman, P. C. Gugelot, D. L. Watson, and C. Fred Moore, Phys. Rev. Lett. **64**, 372 (1990); Phys. Rev. C **42**, 1500 (1990).

[9] D. Ashery, I. Navon, G. Azuelos, H. K. Walter, H. J. Pfeiffer, and F. W. Schlepütz, Phys. Rev. C **23**, 2173 (1981).

[10] R. A. Schumacher, P. A. Amaudruz, C. H. Q. Ingram, U. Sennhauser, H. Breuer, N. S. Chant, A. E. Feldman, B. S. Flanders, F. Khazaie, D. J. Mack, P. G. Roos, J. D. Silk, and G. S. Kyle, Phys. Rev. C **38**, 2205 (1988).

[11] D. J. Mack, Ph.D. thesis, University of Maryland, Maryland, 1987; D. J. Mack, P. G. Roos, H. Breuer, N. S. Chant, S. D. Hyman, F. Khazaie, B. G. Ritchie, J. D. Silk, G. S. Kyle, P.-A. Amaudruz, Th. S. Bauer, C. H. Q. Ingram, D. Renker, R. A. Schumacher, U. Sennhauser, and W. J. Burger, Phys. Rev. C **45**, 1767 (1992).

[12] S. D. Hyman, D. J. Mack, H. Breuer, N. S. Chant, F. Khazaie, B. G. Ritchie, P. G. Roos, J. D. Silk, P.-A. Amaudruz, Th. S. Bauer, C. H. Q. Ingram, G. S. Kyle,

D. Renker, R. A. Schumacher, U. Sennhauser, and W. J. Burger, Phys. Rev. C **41**, R409 (1990).

[13] S. D. Hyman, Ph.D. thesis, University of Maryland, Maryland, 1989; S. D. Hyman, D. J. Mack, P. G. Roos, H. Breuer, N. S. Chant, F. Khazaie, B. G. Ritchie, J. D. Silk, G. S. Kyle, P.-A. Amaudruz, Th. S. Bauer, C. H. Q. Ingram, D. Renker, R. A. Schumacher, U. Sennhauser, and W. J. Burger, to be submitted to Phys. Rev. C.

[14] W. J. Burger, E. Beise, S. Gilad, R. P. Redwine, P. G. Roos, N. S. Chant, H. Breuer, G. Ciangaru, J. D. Silk, G. S. Blanpied, B. M. Preedom, B. G. Ritchie, M. Blecher, K. Gotow, D. M. Lee, and H. Ziock, Phys. Rev. Lett. **57**, 58 (1986); Phys. Rev. C **41**, 2215 (1990).

[15] H. E. Jackson, S. L. Tabor, K. E. Rehm, J. P. Schiffer, R. E. Segel, L. L. Rutledge, Jr., and M. A. Yates, Phys. Rev. Lett. **39**, 1601 (1977).

[16] J. Källne, J. Davis, R. C. Minehart, R. R. Whitney, R. L. Boudrie, J. McClelland, and A. W. Stetz, Phys. Lett. **97B**, 205 (1980).

[17] J. Källne, R. C. Minehart, R. R. Whitney, R. L. Boudrie, J. B. McClelland, and A. W. Stetz, Phys. Rev. C **28**, 304 (1983).

[18] D. Ashery, R. J. Holt, H. E. Jackson, J. P. Schiffer, J. R. Specht, K. E. Stephenson, R. D. McKeown, J. Ungar, R. E. Segel, and P. Zupranski, Phys. Rev. Lett. **47**, 895 (1981), and references therein.

[19] M. Steinacher, G. Backenstoss, M. Izycki, P. Salvisberg, P. Weber, H. -J. Weyer, A. Hoffart, B. Rzehorz, H. Ullrich, M. Dzemidizić, M. Furić, and T. Petković, Nucl. Phys. **A517**, 413 (1990), and references therein.

[20] P. Weber, J. McAlister, R. Olszewski, A. Feltham, M. Hanna, R. R. Johnson, M. Pavan, C. Ponting, F. M. Rozon, M. Sevior, V. Sossi, D. Vetterli, D. Humphrey, G. J. Lolos, Z. Papandreou, R. Tacik, D. Ottewell, G. Sheffer, G. R. Smith, Y. Mardor, and S. May-Tal, Phys. Rev. C **43**, 1553 (1991).

[21] H. Yokota, K. Nakayama, K. Ichimaru, T. Katsumi, T. Mori, S. Igarashi, K. Hama, R. Chiba, K. Nakai, J. Chiba, H. En'yo, S. Sasaki, T. Nagae, and M. Sekimoto, Phys. Rev. Lett. **57**, 807 (1986).

[22] T.-S. H. Lee and K. Ohta, Phys. Rev. Lett. **49**, 1079 (1982).

[23] K. Ohta, M. Thies, and T.-S. H. Lee, Ann. Phys. (N.Y.) **163**, 420 (1985).

[24] J. A. Niskanen and A. W. Thomas, Phys. Lett. B **196**, 299 (1987).

[25] Yke Lefevere, Jan H. M. Bijleveld, Martin Doets, Norbert Idskes, Thomas S. Bauer, Herbert Breuer, and Mahbubul A. Khandaker, Nucl. Instrum. Methods **A290**, 34 (1990).

[26] R. Hamers, Ph.D. thesis, Free University of Amsterdam, The Netherlands, 1989; Th. S. Bauer, R. Hamers, P. Boberg, H. Breuer, R. van Dantzig, F. Geerling, S. Hyman, J. Konijn, C. T. A. M. de Laat, Y. Lefevere, A. Taal, J. L. Visschers, and R. Ykema, submitted to Phys. Rev. C.

[27] R. Brun, F. Bruyant, M. Maire, A. C. McPherson, P. Zanarini, GEANT3, CERN program library, DD/EE/84-1 (1987).

[28] D. F. Measday and C. Richard-Serre, CERN **69-17** (1969).

[29] R. Ent, Ph.D. thesis, NIKHEF-K, Amsterdam, The Netherlands, 1989.

[30] P. G. Roos, L. Rees, and N. S. Chant, Phys. Rev. C **24**, 2647 (1981); N. S. Chant and P. G. Roos, Phys. Rev. C **39**, 957 (1989). The impulse approximation calculations were done using the computer code THREEDEE of N. S. Chant (unpublished).

[31] D. M. Whittal, A. A. Cowley, J. V. Pilcher, S. V. Förtsch, F. D. Smit, and J. J. Lawrie, Phys. Rev. C **42**, 309 (1990).

[32] B. Brinkmöller, C. L. Blilie, D. Dehnhard, M. K. Jones, G. M. Martinez, S. K. Nanda, S. M. Sterbenz, Yi-Fen Yen, L. G. Atencio, S. J. Greene, C. L. Morris, S. J. Seestrom, G. R. Burleson, K. S. Dhuga, J. A. Faucett, R. W. Garnett, K. Maeda, C. Fred Moore, S. Mordechai, A. Williams, S. H. Yoo, and L. C. Bland, Phys Rev. C. **44**, 2031 (1991); B. Brinkmöller and D. Dehnhard, private communication.

[33] E. Oset, Y. Futami, and H. Toki, Nucl. Phys. **A448**, 597 (1996).

[34] M. Thies, Lecture at Les Houches Winter School on Nuclear Matter and Heavy Ion Collisions, 1989 (unpublished).

[35] M. Baumgartner H. P. Gubler, G. R. Plattner, W. D. Ramsay, H. W. Roser, I. Sick, P. Zupranski, J. P. Egger, and M. Thies, Nucl. Phys. **A399**, 451 (1983).